Jour. of the KGS, Vol. 20, No. 7. September 2004, pp. 171~181

Modeling of the Tensile Strength of Unsaturated Granular Soil Using Soil-water Characteristic Curve

흙-수분 특성 곡선을 이용한 불포화모래의 인장강도 모델링

Kim, Tae-Hyung[1] 김 태 형
Kim, Chan-Kee[2] 김 찬 기
Kim, Tae-Hoon[3] 김 태 훈

요 지

본 연구는 불포화 상태 전 범위에 대한 사질토의 인장강도 모델화 가능성을 조사하기 위해 실시 되었다. 새로 개발된 직접인장시험기법을 이용하여 인장시험이 실시되었다. 측정된 결과는 Rumpf 및 Schubert가 동일크기의 이상적인 구에 대해 개발한 이론적인 인장강도 모델들에 의한 예측 값과 비교 되었다. 이를 위해 석션-포화실험을 통해 얻어진 흙-수분특성곡선을 이용하여 이론모델에 있어 중요한 요소인 불포화상태(pendular, funicular, capillary) 구분 및 음의 간극수압 값을 산정하는데 사용하였다. Pendular 상태에서 불포화모래의 비선형 거동이 Rumpf의 모델에 의해 적절이 묘사되었다. Funicular 및 capillary상태의 경우, 함수비가 증가함에 따라 인장강도가 증가하다 최고 값이 도달한 후 다시 감소하는 실험 측정치의 경향도 Schubert의 모델에 의해 적절히 묘사되었다. 본 비교 연구는 이상적인 단일 크기의 입자에 대해 개발된 이론적인 모델이 다양한 크기를 갖는 불포화 사질토의 인장강도를 예측할 수 있다는 가능성을 뒷받침해준다.

Abstract

This study was conducted to explore the tensile strength models in granular soil at the full range of unsaturated state. Direct tension experiments were carried out with a newly developed direct tension technique. The measured experimental data were compared with theoretical models developed by Rumpf and Schubert for monosized ideal particulate solids at the unsaturated state. To do this, the soil-water characteristic curve obtained from a suction-saturation experiment was used to define the unsaturation state and the negative pore water pressure with different water content levels, which are important factors in theoretical tensile strength models. The nonlinear behavior of the tensile strength for unsaturated granular soil at the pendular state is appropriately simulated with Rumpf's model. For the funicular and capillary states, the predicted trend by Schubert's model is properly matched with the experimental data: tensile strength steadily increases and reaches a maximum value and then decreases until it reaches zero. This comparison supports the concept that the tensile strength of unsaturated real granular soil can be approximately simulated with theoretical models.

Keywords : Soil-water characteristic curve, Suction-saturation, Tensile strength, Unsaturated state

1 Member, Full Time Instructor, Division of Civil and Environmental Engrg., Korea Maritime Univ. (kth67399@hotmail.com)
2 Member, Associate Prof., Dept. of Civil Engrg., Dajin Univ.
3 Member, Ph.D., Associate Researcher, DAEWOO E&C

1. Introduction

In geotechnical engineering practice, it is generally assumed that sandy soils exhibit only shear strength and insignificant or no tensile strength (and cohesion) which is generally true for dry or fully saturated and drained sandy soils. It is for these conditions (dry or saturated) that most laboratory data exist. In view of these considerations, investigations of the tensile behavior of sand have not received much attention, and the vast majority of analysis methods and numerical models dealing with sands consider only the compressive strength of the soil mass and take the tensile strength and cohesion to be equal to zero.

However, in the field, perfectly dry soils seldom occur, and moist near-surface deposits are frequently located above the water table and exist in an unsaturated rather than fully saturated state. It is exactly these unsaturated soils that comprise the vast majority of normal construction environments, and thus these factors should be of special concern. Experimental and theoretical investigations for unsaturated soils have been conducted widely over the past couple of decades (Fredlund and Rahardjo, 1995; Cho and Santamarina, 2001). Most researches have focused mainly on the volume change, flow, and shear strength of the unsaturated fine-grained soils. Several models also have been proposed to empirically predict the permeability and the shear strength for an unsaturated soil from the soil-water characteristic curve (Fredlund et al., 1994, 1996; Rahardjo and Fredlund, 1995). However, investigations of tensile strength of unsaturated soils, especially sandy soils, have not received much attention except for cemented soils and clayey soils (Fang and Chen, 1971; Al-Hussaini and Townsend, 1973; Yong and Townsend, 1981; Mikulitsch and Gudehus, 1995). Consequently, due to the lack of data regarding tensile strength on granular soils, little or no emphasis has been given to modeling study that can predict tensile strength.

The objectives of this paper are to investigate a theoretical tensile strength model developed for mono-sized particulate solids at the unsaturated state and to examine its application to a real granular material having a variety of particles. To achieve these objectives, the soil-water characteristic curve obtained from a suction-saturation experiment is used to define the unsaturation state and the negative pore water pressure with different water content levels.

2. Theoretical Studies

2.1 Capillary Forces

Capillary forces induced by water can substantially control the properties and behavior of an assembly of solid particles. Even at low moisture contents, small amounts of water form water-bridges at contact points, and as the water content increases these bridges become larger and more developed resulting in capillary bonding between particles, giving rise to both cohesion and tensile strength.

Capillary bonding generally leads to two force components at low water content levels (in the pendular state which is defined as the state where the water is disconnected except for the very thin films of water surrounding the solids): 1) the surface tension force acting along the water-particle contact line (F_s), and 2) the force due to the difference in the pressures outside and inside the bridge acting on the cross-sectional area (F_c). The surface tension tends to force the particles together, whereas the force due to the pressure difference can only contribute to particle adhesion if there is a net pressure deficiency within the bridge. Due to the presence of water-bridges between the particles, these two forces act together as a total bonding force (F_t).

The total component of inter-particle force (F_t) caused by water-bridge in an ideal soil was originally proposed by Fisher in the 1920s. Rumpf (1961), Schubert et al. (1975), Schubert (1984) and Pierrat and Caram (1997) developed and determined theoretically the magnitude of the capillary bonding forces, F_t, F_s, and Fc in a mono-sized sphere in the pendular state. For instance, if a water bridge exists between two particles of diameter (d) and separated by a distance (a) as shown in Fig. 1, the surface tension for the liquid (F_s) is given in a dimen-

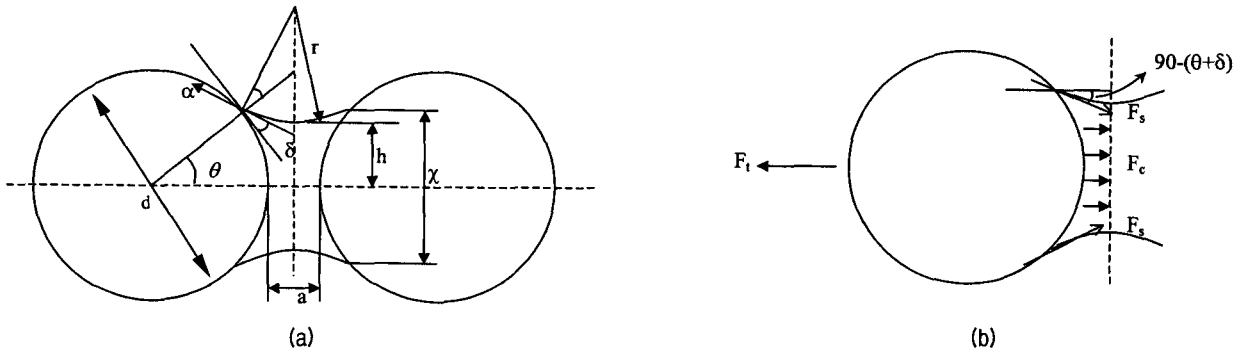

Fig. 1. (a) Water-bridge bonding two monosized spherical particles (From Pierrat and Caram, 1997) and (b) One-dimensional free-body diagram of bonding forces

sionless form as

$$\frac{F_s}{\alpha d} = \pi \sin\theta \sin(\theta+\delta) \tag{1}$$

where θ is the filling angle, and α and δ are the surface tension and contact angle, respectively. The force (F_c) is due to the difference of the pressure within the bridge acting on the cross-sectional area and is also given in a dimensionless form as

$$\frac{F_c}{\alpha d} = \pi\left(\frac{\sin\theta}{2}\right)^2\left(\frac{1}{r^*}-\frac{1}{h^*}\right)$$
$$h^* = \frac{h}{d} = \frac{\sin\theta}{2} + \frac{r}{d}\left[\sin(\theta+\delta)-1\right]$$
$$r^* = \frac{r}{d} = \frac{(1-\cos\theta)+a/d}{2\cos(\theta+\delta)} \tag{2}$$

where h^* and r^* are the two dimensionless radii of curvature of the water bridge, when taken as arcs of a circle. The total dimensionless bonding force (F_t) is the sum of the two components as a function of the contact and filling angles (δ and θ) and the dimensionless separation distance (a/d).

$$\frac{F_t}{\alpha d} = \pi \sin\theta\left[\sin(\theta+\delta) + \frac{\sin\theta}{4}\left(\frac{1}{r^*}-\frac{1}{h^*}\right)\right] \tag{3}$$

The contributing dimensionless forces (F_s and F_c) and the resulting dimensionless total force (F_t) as a function of the filling angle with a/d = 0.025 and complete wetting ($\delta = 0°$) are shown in Fig. 3. As the filling angle increases, the contact line length of the water-particle contact increases and results in increasing the attraction force (F_s), which is the product of this length with the surface tension of the wetting liquid. However, the pressure-induced force (F_c) reaches a maximum at the filling angle of 20°, and as the filling angle increases, F_c starts decreasing, eventually becoming negative, and indicating a repulsive force. While this may seem counterintuitive since the capillary pressure remains negative until the assembly of particles is fully saturated, the result can be explained by the relative size of the two dimensionless radii of curvature, h^* and r^*. As the size of the water-bridge grows, h^* increases faster than r^* and eventually becomes larger. The net resulting dimensionless total force would be a positive value that increases sharply with water content at low filling angle and leveling off as the water content is further increased.

2.2 Tensile Strength Models

Rumpf (1961) proposed the theory of tensile strength for agglomerates at the pendular state.

$$\sigma_{tp} = \frac{(1-n)}{n}\frac{F_t}{d^2} \tag{4}$$

However, the interaction between water and particles in unsaturated granular materials is actually changed with increasing water content inside. That is, the capillary forces arising from the bridge bonding system gradually diminish as the water content increases. Figure 2 shows the states of saturation in unsaturated soils. In the capillary state, which is defined as the state where the pores are completely filled with the water, the capillary

forces originating from the interfacial forces exist only at the surface agglomerate and a negative capillary pressure develops in the interior, rather than the bridge bonding systems. In 1984, Schubert proposed a tensile strength model in the capillary state.

$$\sigma_{tc} = S \cdot P_c \tag{5}$$

where S is the degrees of saturation, P_c is the capillary pressure. The saturation amount is related to the water content, porosity and specific gravity of solids by the following relation:

$$S = \frac{1-n}{n} G_s w \tag{6}$$

In the funicular state (see Fig. 2 (b)), which is defined as the state where both water-bridges and pores filled with the water present, therefore, both capillary forces due to water-bridges and regions filled with water contribute to the total bonding. Schubert also proposed the tensile strength in which both bridge bonding and bonding caused by regions filled with water contribute

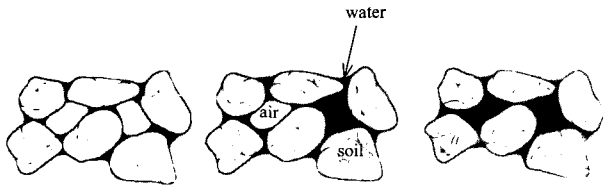

(a) pendular state (b) funicular state (c) capillary state

Fig. 2. States of saturation in unsaturated granular materials (From Schubert et al., 1975)

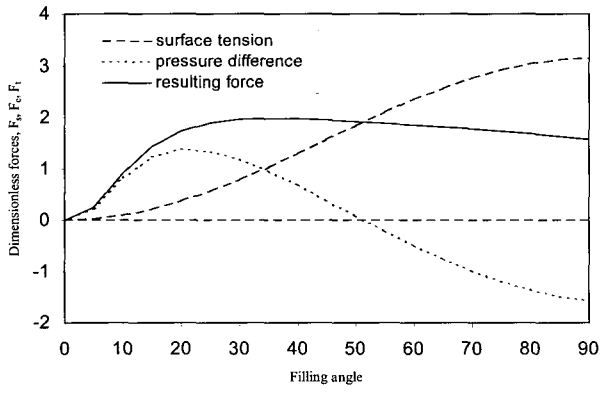

Fig. 3. Dimensionless bonding forces as a function of the filling Angle (θ) for a/d = 0.025 and δ = 0°

to the tensile strength according to their proportions.

$$\sigma_{tf} = \sigma_{tp} \frac{S_c - S}{S_c - S_f} + \sigma_{tc} \frac{S - S_f}{S_c - S_f} \tag{7}$$

where σ_{tp} and σ_{tc} are the tensile strengths for the pendular and the capillary states, which are computed from Eqs. 4 and 5, respectively. S_c and S_f are the upper saturation limits for the funicular and pendular states, respectively. The values of S_f and S_c are taken from the soil-water characteristics curve (SWCC).

3. Direct Tension Experiments

3.1 Apparatus

The device consists of a split acrylic box with an open top (Kim, 2002b). One half of the specimen box is secured to the guide rails, thus fixing it in place, while the other half is free to slide on linear bearings that ride on machined guide rails. The system for applying the loads to the specimen is very straightforward. Two containers are attached to the movable half of the container and suspended from a wire and pulley system, one container to the front and the other to the rear. To impose load on the failure surface in this load-controlled apparatus, water is added to the front container very slowly. Because of concerns about slippage of the specimen along the vertical boundaries where the normal stresses could be quite low, triangular wooden wedges were added to the side walls. These wedges were covered with sandpaper to allow them to engage the sand specimens without slippage. These blocks had the added advantage of acting to force a highly vertical, flat failure surface along the split between the container halves (See Fig. 4 (a)).

Direct measurement of negative pore water pressure is ideal, but its device has not been added in this system. So, soil-suction tests were conducted instead in order to measure the suction value.

3.2 Analysis of Stress State in Apparatus

The majority of the applied horizontal force will be

transferred to each half of the specimen through normal stresses (σ_x) and shear stresses (τ) on the rough surfaces of the wedges, as shown in the sketch below (Fig. 4 (b)). Some force may be applied through shear stresses on the floor of the split box, but this is likely to be substantially less than the forces transmitted along the wedge surfaces AC and BD.

Assuming that all the applied force (F) is transmitted to the sand specimen via stresses on the surfaces of the wedges, resolving in the x-direction gives :

$$F = 2h\int_0^L (\sigma_n \sin\alpha + \tau\cos\alpha)dl = \bar{\sigma}_x hd \tag{8}$$

Where h is the height of the specimen in the z-direction, α is the angle of the wedges, l is the inclined distance along the wedge surface (of total length L) and $\bar{\sigma}_x$ is the mean value of tensile stress in the x-direction on the failure plane AB. But $dll\cos\alpha = dx$, and if δ_m is the mobilized friction angle on the wedge surface ($\tan\delta_m = \tau/\sigma_n$) then Eq. 8 can be re-written as :

$$2\int_0^X \sigma_n(\tan\alpha + \tan\delta_m)dx = \bar{\sigma}_x d \tag{9}$$

where X is the length of each half of the split-box in the x-direction. Assuming the mobilized friction angle δ_m is constant along the surfaces of the wedges, Eq. 9 becomes :

$$2(\tan\alpha + \tan\delta_m)\int_0^X \sigma_n dx = \bar{\sigma}_x d \tag{10}$$

Resolving in the y-direction, if $\bar{\sigma}_y$ is the mean value of compressive stress in the y-direction on any vertical plane, such as EF, that is perpendicular to the failure plane AB :

$$\bar{\sigma}_y hX = h\int_0^L (\sigma_n\cos\alpha - \tau\sin\alpha)dl \tag{11}$$

Using $dll\cos\alpha = dx$ and $\tau/\sigma_n = \tan\delta_m$ again :

$$\bar{\sigma}_y X = h\int_0^X \sigma_n(1-\tan\alpha\tan\delta_m)dx \tag{12}$$

Again assuming that δ_m is constant, Eq. 12 becomes :

$$\bar{\sigma}_y X = (1-\tan\alpha\tan\delta_m)\int_0^X \sigma_n dx \tag{13}$$

Combining Eqs. 10 and 13 gives :

$$\bar{\sigma}_y = \frac{(1-\tan\alpha\tan\delta_m)}{(\tan\alpha+\tan\delta_m)}\frac{d}{2X}\bar{\sigma}_x \tag{14}$$

This apparatus was developed as a uniaxial tension

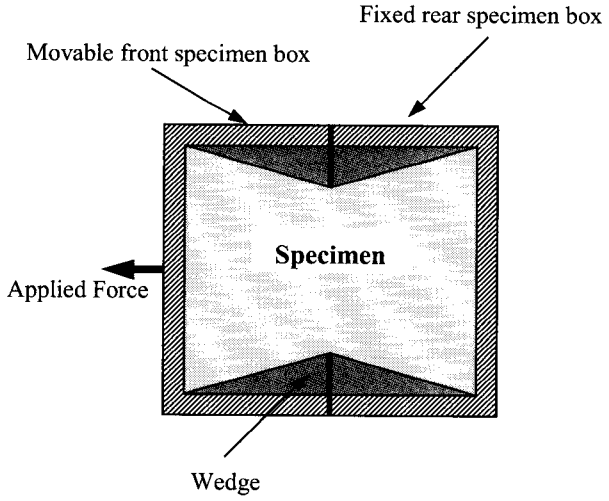

(a) Plan view of specimen

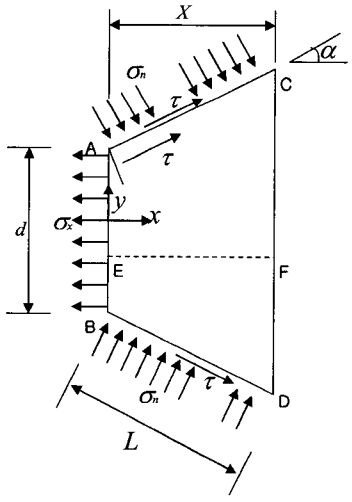

(b) Stress state in specimen

Fig. 4. Direct tension box

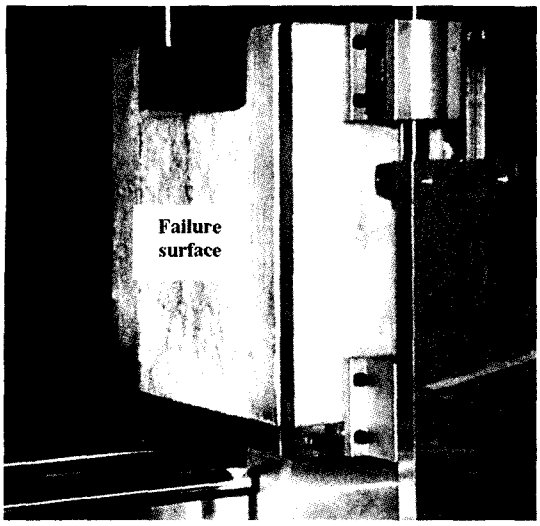

Fig. 5. Photograph of vertical sand face, roughly 170 mm high

test, where the applied axial tensile stress is one principal stress and the other two mutually perpendicular principal stresses are zero. However, there is a certain amount of compressive principal stress (σ_y) acting in the perpendicular horizon-direction as shown in Eq. 14. In addition, there is vertical compressive stress (σ_z) caused by the weight of the sand which increases with depth below the sand specimen surface. The stress state in the failure region (see Figs. 4 and 5) is therefore actually 3-dimentional, with one tensile principal stress and two compressive principal stresses. The measured value of tensile strength may well have been affected by the presence of two perpendicular compressive principal stresses, but this situation was not considered in this experiment.

3.3 Specimen Preparation

All specimens were prepared using F-75 Ottawa silica sand, which is a fine-grained natural quartz sand of uniform gradation with a mean particle size of 0.22 mm. It has a specific gravity of 2.65, maximum and minimum void ratios of 0.805 and 0.486, respectively. Two categories of sand mixtures were prepared for the experiments to study the effect of fines on the tensile strength. The first version of the sand (F-75-C) was prepared by washing through a No. 200 sieve to remove particles smaller than 0.075 mm. A second version (F-75-F) was prepared by adding 2.0% fines by weight.

Table 1. Experimental program for direct tension experiments

Material type	F-75-C (free of fines)	F-75-F (2% of fines)
Relative density (%)	50%	50%
Water content (%)	0.5	0.5
	1.0	1.0
	2.0	2.0
	4.0	4.0
	5.0	5.0
	8.0	8.0
	11.0	11.0
	15.0	15.0
	18.0	18.0

The reason for selecting a 2% of fines is that the inclusion of small amounts of fines, which may be produced by tumbling and abrasion of sand in the field, especially the wearing down of sharp edges, remains a concern regarding defining proper engineering properties of F-75 sand. Table 1 shows the full testing program, and experiments were only conducted to water contents of 18% due to the limitation of test apparatus.

3.4 Experimental Procedure

Prior to beginning each experiment, the two halves of the box were secured by taping them together with cellophane tape. The loading container and counterbalance container were then attached. The specimen was then prepared at the desired moisture content and density. During this process, care was taken to use thin plastic wrap and a water-misting bottle to prevent drying of the sand specimen surface.

Immediately prior to loading the sand in tension, the cellophane tape was cut along the seam between the two halves of the box. The load was then slowly and steadily applied by introducing water to the loading container at a rate of about 0.03 N/sec. The load was steadily increased until failure occurred, and the load was then measured by taking the mass of the water added to the loading container. The error in load-mass measurement was ± 0.01 g. The moment of failure was very apparent, as the two container halves parted rapidly, leaving a nearly vertical standing face of sand along the failure surface (Fig. 5).

Immediately following failure, the mass, and thereby the density, of the specimen were determined by placing the entire apparatus on a large scale. The majority of the specimen was then quickly dug out of the box and immediately weighed for the determination of moisture content. The tensile strength of the sand was computed by dividing the applied load by the cross-sectional area of the failure surface.

A more detail information of the tensile experiments is described in Kim's papers (2002a, 2002b).

4. Results and Analysis

4.1 Effect of Water Content

The results of the experiments on F-75 sand are shown in Fig. 6. The tensile strength steadily increases for water contents in the range of 4~10%. For water contents in the range of 10~15%, the tensile strength keeps increasing with a slightly steeper slope and eventually reaches a maximum value (σ_t = 1.6 kPa) at a water content of 15%. Beyond this point, the tensile strength dramatically decreases as the water content increases. It would be expected that the tensile strength would eventually decay to near zero as the water content approached saturation, but data indicate only to a water content of 18%.

At low water levels, water-bridges form at the particle-particle contact points. This results in capillary bonding forces between the particles, which lead to a certain amount of tensile strength in the soil. As the water level increases, the water-bridges become more developed in the contact geometries, and the tensile strength increases. As the water content keeps increasing, the bonding forces developed by the bridge system gradually disappear, whereas the interfacial tension forces at the surface of the agglomerate and a negative capillary pressure in the interior of this agglomerate develop as a new capillary bonding force (Schubert, 1984). The magnitude of tensile strength is decided by summing up these two bonding forces, and the peak tensile strength can be assessed when the combination of these bonding forces reaches a maximum level.

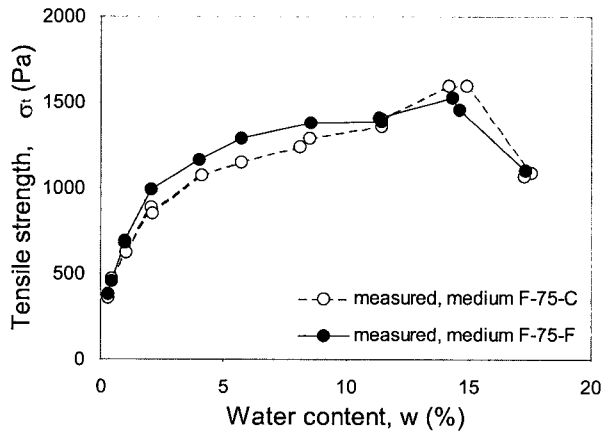

Fig. 6. Results of direct tension testing: tensile strength versus water content

4.2 Effect of Fines

Figure 6 also indicates that the initial slope of the regression curve for the F-75-F sand is a little bit steeper than that of the F-75-C sand. This trend continues until the water content up to 11% is reached. Beyond this point of the water content, however, the trend is reversed: the tensile strength of the F-75-C sand is a little bit higher than that of the F-75-F sand.

At low water content levels, fines offer additional bonding in structure resulting from surface tension and capillary pressure of water-bridges, which are constructed at contact points between the particles, because fine particles contribute to increase the contact points and the capillary potential. The contribution of fines on the tensile strength continues until the water content reaches a certain point at around 11%. When the water content passes this point, the bonding forces contributed by fines vanish, and the fines help to lose the contacts and act more like lubrication so that the results obtained from the F-75-F sand show low tensile strength at high water content levels. This result clearly shows that the fines effects are greatly influenced by the water content. In addition, as seen in Fig. 6, the effect of fines on tensile strength is small from a practical perspective.

5. Soil-Water Characteristic Curve (SWCC)

In order to apply the theoretical tensile strength models developed by Rumpf and Schubert, a suction-saturation experiment is first required to define the saturation state and the capillary pressure with different water content levels as mentioned in Section 2.

A suction-saturation test based on the flow pump technique was thus conducted on F-75-C with medium relative density (D_r = 50%) by using the technique. This flow pump technique was originally introduced by Olsen (1966) to improve the measurement method of the saturated hydraulic conductivity. Then, Znidarčić and his students at the University of Colorado at Boulder adopted a similar flow pump technique in the development of a new method for the measurement of the Soil Water Characteristic Curve (SWCC) (Znidarcic et al., 1991). It is a faster, more convenient, and more accurate way of determining the SWCC. The equipment consists of a modified conventional triaxial cell, a differential pressure transducer, the ceramic porous plate (high air entry value porous stone), the flow pump, and the data acquisition system. The height of the sand specimen was 30 mm with a diameter of 71 mm. A more detailed information of the tensile experiments is described in Hwang and Kim's papers (2003, 2004).

The test result is shown in Fig. 7, which indicates the S_c and S_f corresponding to the upper saturation limits for the funicular and pendular states. The upper limit of pendular state (S_f) is clearly defined and easily captured

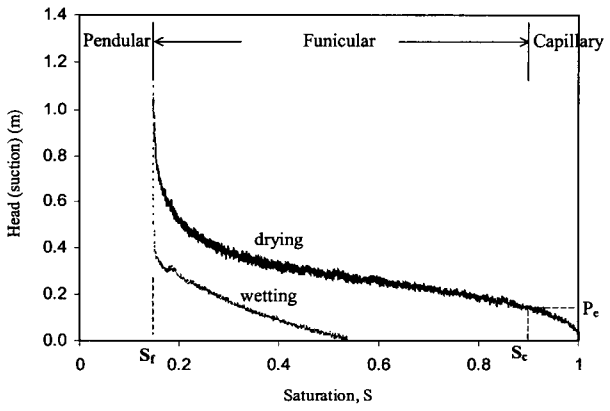

Fig. 7. Soil-water characteristic curves of F-75-C medium granular soil

in the SWCC for both wetting and drying curves. It indicates the saturation levels at about 0.15, which corresponds to about 3.7% water content for medium relative density (D_r = 50%). The value (S_c = 0.9) was selected from the drying curve of the SWCC by selecting the saturation level corresponding to the air entry point (P_e), which is defined as the suction required to force air through an initially water saturated sample. The value (S_f) was clearly defined and easily captured in the curves, whereas the S_c value was determined approximately, because the dry curve is quite flat at higher saturation levels. This is due to the pore-size of soil. In the case of uniform sand such as F-75 sand, all pores and pore channels are of comparable size and shape, thus all pore channels have almost the same capillary suction capacity and the soil water characteristic curve is rather flat. For the wetting curve, the value of S_c could not be defined, because the occluded air bubbles or entrapped air pockets exist within the pore space having no connection over macroscopic distances at a high level of saturation on the wetting curve.

Thus, the tensile strengths were predicted using only the drying curve of the SWCC: in the range of $0 < S < 0.15$ (in the pendular state), the predicted values were computed by Rumpf's model (Eq. 4), in the range of $S > 0.9$ (in the capillary state), the values were predicted by Schubert's model (Eq. 5), and in the funicular state ($0.15 < S < 0.9$), Eq. 6 was used to compute the values of prediction.

6. Comparison between Measured Data and Models

To compute the model's values, the cubical-tetrahedral packing configuration (mean coordination number, k = 8 and e = 0.65) was selected which is a reasonable assumption because the void ratio tested with medium specimens in the experiment is about 0.65. The average particle size of d = 0.22 mm was used in the grain size distribution curve (Kim, 2002b), and the contact angle (δ) was assumed to be zero. In practice, no absolutely smooth particles are found so that the case a/d = 0

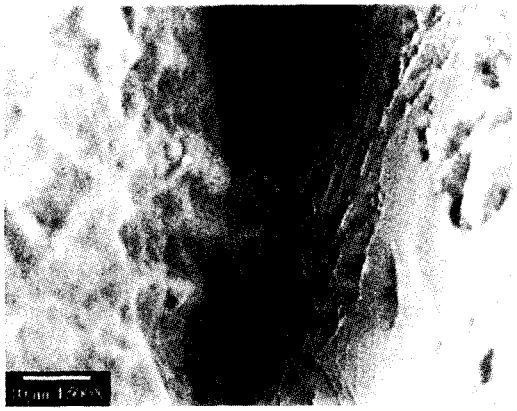

Ottawa 10μm 1500x

Fig. 8. Electron microscope scan image of F-75 granular soil

seldom occurs in a real granular material (d is the diameter of particles and a is the separation distance between particles in Fig. 1). Pierrat and Caram (1997) suggested that values of a/d in the range of 0.005~0.05 are more appropriate instead. This assumption can be assured by an electron microscope scan image of clean F-75 Ottawa soil presented in Fig. 8, which shows that even though this granular material is clean, it has numerous cracks, ridges and fissures on its surfaces. Thus, it does not make sense to use a/d = 0 in the computation. Thus, several values of a/d (0.005, 0.015, 0.025) were used for simulating the experimental data in this study as shown in Fig. 9.

6.1 Pendular State

The predicted tensile strength with Rumpf's model for a/d = 0.005 sharply increases at low saturation levels and a plateau value. The model overpredicts and does not simulate the pattern of the data, because the measured tensile strength steadily increases as the saturation levels increases. For another separation distance, a/d = 0.015, the curve does not really fit the data. The curve still shows a sharp increase of the tensile strength at low saturation levels and a plateau value for the rest of pendular state. This trend was observed for the tensile strength experiments using glass beads (Pierrat and Caram, 1997). However, for a larger separation distance a/d = 0.025, the curve moves downward especially at low

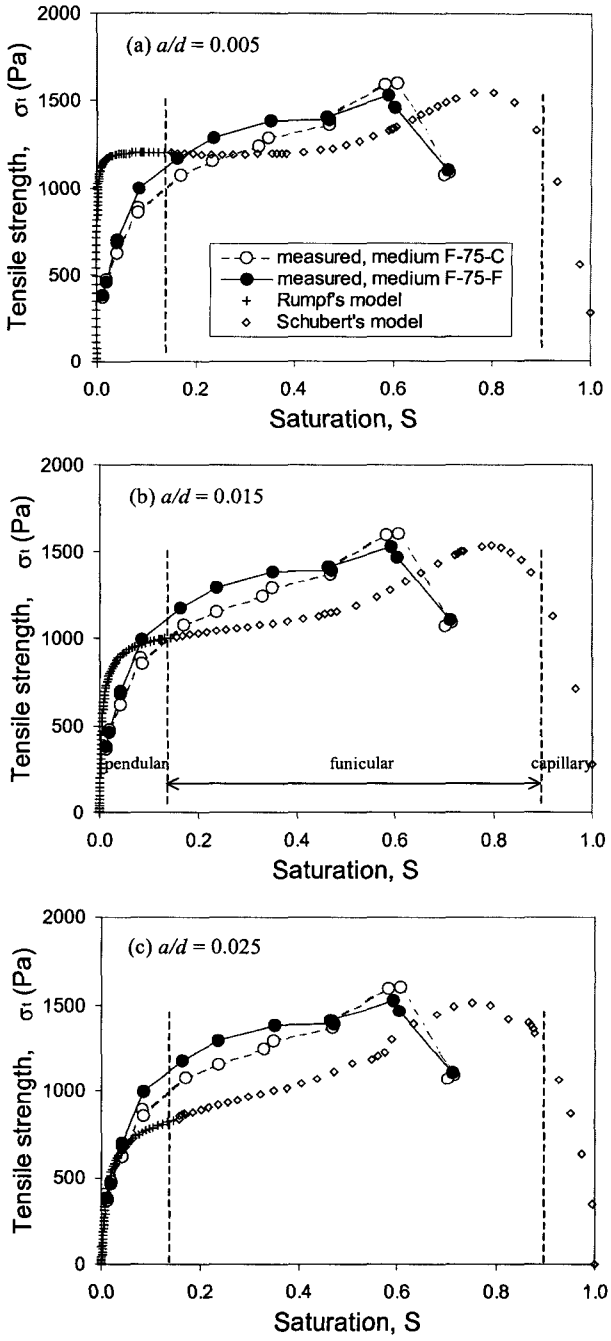

Fig. 9. Comparison of tensile strength between measured and predicted by Rumpf's and Schubert's models

saturation levels and makes it lie closer to the experimental trend (nonlinear behavior), though at higher saturation levels in the pendular state, the curve underpredicts the experimental data.

6.2 Funicular and Capillary States

A prediction was made by Schubert's models with real

values of capillary pressure obtained from the drying in the range of $S > 0.15$. As shown in Fig. 6, the measured tensile strength steadily increases for saturation levels in the range of 0.15~0.6, and then starts to decrease as the saturation increases. It would be expected that the tensile strength would eventually decay to near zero in the fully saturation state ($S = 1$).

For all values of a/d (0.005, 0.015, 0.025), the predicted trend is a good match with the experimental data: tensile strength steadily increases and reaches a maximum value and then decreases until it reaches zero. This trend was expected, because the capillary pressure devised for the drying curve (see Fig. 7) was used in this analysis. However, the model underpredicts in the range of $0.15 < S < 0.6$ and overestimates in the range of $S > 0.6$. Also, the model predicts a maximum tensile strength at saturation level about $S = 0.8$ rather than $S = 0.6$. However, the predicted maximum tensile strength is the same as the experiment value. This comparison between the experimental data and the predicted values supports that the tensile strength of unsaturated granular soil can be approximately simulated with Schubert's model

7. Conclusions

The purpose of this study is to explore the tensile strength models in quartz granular soil at the full range of unsaturated state, which is a pendular, funicular, and capillary state. The experimental data were compared with the values predicted by theoretical models developed by Rumpf and Schubert for unsaturated particulate solids, and its application was discussed for real granular soils. The following conclusions can be drawn.

(1) The measured tensile strength of unsaturated sands is significantly different from zero, and it generally increases with increasing water content and eventually reaches a maximum value at certain water content, and then it decreases. The presence of fines changes the degree of bonding action between the particles, but its influence on the tensile strength is substantially dependent on the water content levels.

(2) For the pendular state, the observed nonlinear behavior of unsaturated granular soils is appropriately simulated with Rumpf's model using a higher value of dimensionless separation distance (a/d), which is a fitting parameter.

(3) For the funicular and capillary states, in comparison with the measured data, the Schubert's model underpredicts in the range of $0.15 < S < 0.6$ and overestimates in the range of $S > 0.6$, but the predicted trend and the magnitude of the maximum tensile strength are a good match with the experimental data for all values of dimensionless separation distance (a/d).

(4) This study supports the concept that the tensile strength of unsaturated real granular soils can be approximately simulated with theoretical models developed for monosized ideal spheres.

References

1. Al-Hussaini, M. M. and Townsend, F. C. (1973), *Tensile testing of soils, a literature review*, U.S. Army Engineer Waterways Experiment Station.
2. Cho, G. C. and Santamarina, J. C. (2001), "Unsaturated particulate materials-particle-level studies", *Journal of Geotechnical and Geoenvironmental Engineering*, Vol.127, No.1, pp.113-144.
3. Fang, H. Y and Chen, W. F. (1971), "Further study of double-punch test for tensile strength of soils", *Proceeding of the Third Southeast Asian Conference on Soil Engineering*, pp.211-215.
4. Fisher, R. A. (1926), "On the capillary forces in an ideal soil: correction of formulas by Haines, W. B.", *Journal of Agriculture Science*, Vol.16, pp.492-505.
5. Fredlund, D. G., Xing, A., and Huang, S. (1994), "Predicting the permeability function for unsaturated soils using the soil water characteristic curve", *Canadian Geotechnical Journal*, Vol.31, pp. 533-546.
6. Fredlund, D. G and Rahardjo, H. (1995), *Soil mechanics for unsaturated soils*, John Wiley & Sons, Inc., New York.
7. Fredlund, D. G., Xing, A., Fredlund, M. D., and Barbour, S. L. (1996), "The relationship of the unsaturated soil shear strength to the soil water characteristic curve", *Canadian Geotechnical Journal*, Vol.32, pp.440-448.
8. Hwang, C. and Kim, T.-H. (2003), "Determination of the soil-water characteristic curve using the flow pump technique", *Journal of the Korean Geotechnical Society*, Vol.19, No.5, pp.155-162.
9. Hwang, C. and Kim, T.-H. (2004), "Determination of the unsaturated hydraulic conductivity function", *Journal of the Korean Geotechnical Society*, Vol.20, No.3, pp.47-51.
10. Kim, T.-H. (2002a), "Effect of moisture on tensile strength", *Journal of the Korean Geotechnical Society*, Vol.18, No.3, pp.13-21.

11. Kim, T.-H. (2002b), "Experimental investigations on tensile strength on sand at low moisture contents", *Journal of the Korean Geotechnical Society*, Vol.18, No.3, pp.23-31.
12. Mikulitsch, W. A. and Gudehus, G. (1995), "Uniaxial tension, biaxial loading and wetting tests on loess", *Proceedings of 1st International Conference on Unsaturated Soils*. Alonso & Delages (eds), pp.45-150.
13. Pierrat, P. and Caram, H. S. (1997), "Tensile strength of wet granular materials", *Powder Technology*, Vol.91, pp.83-93.
14. Rahardjo, H. and Fredlund, D. G. (1995), "Pore pressure and volume change behavior during undrained and drained loadings of an unsaturated soil", *Proceedings of the 1st International Conference on Unsaturated Soils*, Alonso & Delages (eds), pp.165-170.
15. Rumpf, H. (1961), *The strength of granules and agglomerates, Agglomeration*, W.A. Knepper, (ed), Interscience, New York.
16. Schubert, H., Herrmann, W. and Rumpf, H. (1975), "Deformation behavior of agglomerates under tensile stress", *Powder Technology*, Vol.11, pp.121-131.
17. Schubert, H. (1984), "Capillary forces-modeling and application in particulate technology", *Powder Technology*, Vol.37, pp.105-116.
18. Yong, R.N., Townsend, F.C. eds. (1981), "Laboratory shear strength of soil", *ASTM STP*, No.740, pp.717.
19. Znidarčić, D., Illangasekare, T. and Manna, M. (1991), "Laboratory testing and parameter estimation for two-phase flow problems", *ASCE Geotechnical Special Publications*, Vol.27, pp.1089-1099.

(received on Aug. 24, 2004, accepted on Sep. 24, 2004)